Sixth International Symposium on Marine Propulsors
smp'19, Rome, Italy, May 2019

A Stochastic Approach to Cavitation Inception Prediction

Mehedi Bappy[1], J. Ezequiel Martin[1], Jiajia Li[1], Gustavo C. Buscaglia[2], Pablo M. Carrica[1]

[1]IIHR-Hydroscience and Engineering, The University of Iowa, Iowa City, IA, 52242, USA
[2]Instituto de Ciências Matemáticas e de Computação, Universidade de São Paulo, São Carlos, SP, Brazil

ABSTRACT

A novel methodology for the prediction of cavitation inception based on a probabilistic approach is presented along with a limited validation. The simulation of a cavitating flow is a challenging and evolving area of investigation, complicated by the requirement of accurately solving a complex multiphase flow. However, for many practical applications the prediction of conditions for which cavitation will not occur is just as important. A reliable, physics-based method to predict the likelihood of cavitation events, based on well-established single-phase computation methods, will be a valuable tool. The proposed method uses probability distribution functions (pdf) of pressure fluctuations derived from isotropic homogeneous turbulence (IHT) simulations to characterize the sub-grid pressure of a CFD computation. Probabilistic description of the pressure in the computational cell is then used to estimate the cavitation potential of the flow. Additionally, a simple model of a vortex is used to deterministically correct sub-grid underestimation of the pressure drop at the core of resolved vortices, which is a further improvement to the probabilistic correction implemented.

Keywords

Cavitation inception, computational fluid dynamics.

1 INTRODUCTION

While the concept of cavitation inception is intuitively easy to define as the conditions for which cavitation is first detected, multiple working definitions are possible depending both on how the threshold of detection is defined and which mechanisms (i.e., true cavitation involving mass transfer versus "gaseous" cavitation or expansion of nuclei as response to low pressure regions in the flow) are considered. In the present approach, a probabilistic measure of the number of events per unit time, volume and density of precursor nuclei is used, without further constraints on the threshold for detection, which is case specific.

For cavitation to occur, precursors in the form of bubbles or solid impurities in the flow have to be subject to low enough pressure for a long enough period of time. From a numerical point of view, a deterministic approach requires both the Lagrangian tracking of the precursors as well as a full solution of the pressure field, including its fluctuations. This approach is not feasible with current computational capacities for all but the simplest problems and also impractical since it requires the knowledge of the precursors' initial distribution. The following simplifications are considered to develop the proposed model:

- Precursors are described in an Eulerian framework; moreover they are assumed sufficiently small that can be modeled as passive tracers using a one-way coupling approach; as a first approach, constant levels of precursors' density can be used throughout the domain.
- The flow field is solved using CFD (LES, hybrid Reynolds-averaged Navier-Stokes/Detached Eddy Simulation or even RANS). The gap between the modeled pressure and the "real" pressure is bridged using a probabilistic model of the sub-grid pressure fluctuations as well as a deterministic correction as described below.
- The duration of low pressure events is either determined by the CFD solution (both pressure and turbulence) in a probabilistic approach, or in a deterministic fashion considering the temporal evolution of the solution.

In this paper a summary of the proposed models for correcting the modeled pressure and for accounting for cavitation events is presented, as well as results for two cases for which experimental data is available.

2 MODELS

Models developed based on the LES approach to estimate low pressure fluctuations are presented, as well as a discussion of possible computational approaches to a quantitative measure of frequency of cavitation events in the context of inception observability.

2.1 Probabilistic Model of Pressure Fluctuations

Central to the model is the ability to relate the lowest expected pressure fluctuation at the sub-grid scale to the flow turbulence. The LES approach assumes nearly isotropic conditions at the sub-grid scale, therefore it is a reasonable assumption that the pressure fluctuations at that level will resemble, probabilistically, those of IHT data. It has been shown that pdfs of pressure fluctuation in IHT are only function of the Taylor microscopic Reynolds number $R_\lambda = u'\lambda/\nu$, (Cao et al., 1999), which can be

obtained from LES solutions as a function of the strain rate magnitude *S,* the grid size Δ and the Smagorinsky constant C_s as

$$\epsilon = C_s^2 \Delta^2 S^3, \quad (1)$$

$$u' = C_k^{1/2} \left(\frac{\epsilon \Delta}{\nu}\right)^{1/3}, \quad (2)$$

$$\lambda = u' \left(\frac{15\nu}{\epsilon}\right)^{1/2}, \quad (3)$$

with ν the kinematic viscosity, ϵ the modeled dissipation rate and $C_k \approx 1.5$, the Kolmogorov constant. Alternative definitions can be used if other models are used to simulate the turbulent kinetic energy k and ϵ. To generate a model applicable to numerical solutions, we approximate the pdfs reported by Pumir (1994) and Cao et al. (1999) by a Gaussian with an exponential tail that depends on R_λ towards very negative pressures. As discussed by Ran & Katz (1994), the probability of reaching pressure values *below* a threshold is relevant to inception, i.e., the cumulative probability distribution function (cdf) of the pressure fluctuations. Defining the cdf: $C(z) = Prob(\frac{\Delta P}{\rho u'^2} < z)$, where ΔP is the pressure fluctuation, data-fitting lead to the following expressions:

$$C(z) = \frac{1}{21 R_\lambda^{-0.7}} \exp\left(-6.9 + 21 R_\lambda^{-0.7}(z+5)\right), z \leq = -5$$

$$C(z) = C(-5) + 7.52 \times 10^{-4}\left[\exp\left(1.33(z+5)\right) - 1\right], \quad -5 \leq z \leq -2 \quad (4)$$

$$C(z) = C(-2) + 0.5\left[\mathrm{erf}\left(z/\sqrt{2}\right) - \mathrm{erf}\left(-\sqrt{2}\right)\right], z \geq -2$$

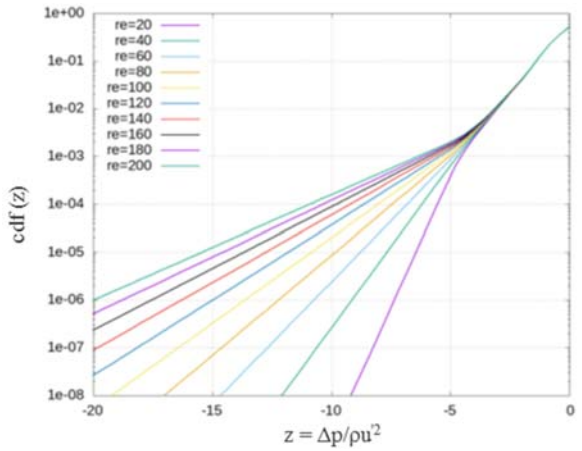

Figure 1: Cumulative probability distribution C(z), given in Eqn. (4), for several Taylor Reynolds number R_λ.

The cdf is also shown graphically in Figure 1. Notice that as R_λ decreases the tail of the pdf becomes steeper and the probability of large negative fluctuations decreases considerably. This has a number of consequences worth noticing. From the definitions of R_λ and Equations (1) through (3), we have that $R_\lambda \sim \Delta S^{1/2}$ and $u' \sim S\Delta$, which reflects the fact that as the grid is refined the correction becomes less important, since both R_λ and the scaling of the dimensionless pressure fluctuations $\rho u'^2$ decrease. Additionally, for a constant grid size, regions with low strain rate are less affected by the model; in particular, as it is shown in §2.2, the probabilistic model has little effect in the core of well resolved vortices.

The approach can in principle be extended to hybrid RANS/LES models with some caveats. The assumption that the sub-grid fluctuations near walls follow IHT data is likely not valid, and should be replaced by an appropriate sub-grid pressure distribution obtained from wall turbulence. Additionally, R_λ is much larger in the near wall regions than available DNS data, which requires an extrapolation of the pdfs for those regions. Finally, regions where the LES model is active should be properly discretized such that the results are comparable to a formal LES simulation, since DES approaches a Smagorinsky closure in LES regions (Spalart 1999). Regardless of these shortcomings, the model should produce acceptable results in the regions where the model is fully valid, providing better estimations of the pressure fluctuations in the RANS regions of the simulation while drastically reducing the number of required points needed to simulate complex geometries such as a propeller. In RANS regions, including full RANS simulations, the correction should be interpreted as a "modeled" correction rather than a sub-grid/unresolved addition, and as such, there are possibly different expressions than those in Eqn. (4) that can provide more accurate predictions. Work is on-going to validate this hypothesis.

2.2 Deterministic Model of Pressure Defect in Vortices

The probabilistic model discussed in §2.1 does not address the under-prediction of the pressure field at the center of resolved vortex due to grid discretization. Furthermore, the probabilistic correction depends on the magnitude of the strain rate, but in the vortex core S is negligible and thus is also the correction.

To generate a mechanistic model of resolved vortices, we take a local coordinate system with θ and r the azimuthal and radial coordinates, respectively, so that the pressure gradient and azimuthal velocity are approximately related by

$$\frac{dP}{dr} = \frac{u_\theta^2}{r} = \Omega^2 r f(r), \quad (5)$$

where f is a function of the vortex model used to relate the vorticity and the tangential velocity (for instance, f=1 for a Rankine vortex) and Ω the rotational rate. Integrating and evaluating at the grid size we obtain

$$\Delta P = \frac{1}{2}\Omega^2 r^2 F(r) \cong max(Q,0) h^2 F(h), \quad (6)$$

where h is the grid cell size, F a function of the vortex model, and $Q = 1/2\,(\boldsymbol{\Omega}^2 + \boldsymbol{S}^2)$, with $S = \sqrt{2\boldsymbol{S}^2}$. The approximation is valid in the regions of interest, as S is

negligible in the core, and by using positive valued Q-criterion it restricts the correction to the resolved vortices. The formulation is again such as to obtain F=1 for a Rankine vortex.

Thus far we have a simple correction to the total pressure field, $P_{\mathrm{Corr}} = P_{\mathrm{LES}} - \Delta P$ but the correction fails to address grid dependency because Q also depends on the grid resolution. The details of the calculation are not shown for brevity, but it can be demonstrated that based on a Lamb-Oseen vortex model and restricting some variables to be consistent with the grid size, the pressure correction by poor resolution at vortex cores is

$$\Delta P \cong max(Q,0)\, h^2 F(h) e^{2min\{[2h/(max(a,h+d)]^2,2\}} \quad (7)$$

with a and d, respectively the vortex core radius and the local coordinate value of r estimated as

$$d = \frac{|\nabla P|}{max(Q,\varepsilon)} \quad (8)$$

$$a = \sqrt{\frac{4\, max(d,h/2)\, max(Q,\varepsilon)}{max(|\nabla Q|,\varepsilon)}} \quad (9)$$

with $\varepsilon \sim 10^{-6}$ to prevent division by zero. To the resulting corrected pressure a probabilistic correction can be further added based on the model described in the previous section.

Figure 2 illustrates the effect of the deterministic correction on the pressure pdfs of the Schiebe body presented in §3.1. Once corrected, the tail of the pressure distribution is comparable for all grids, while the uncorrected pressure is strongly grid dependent.

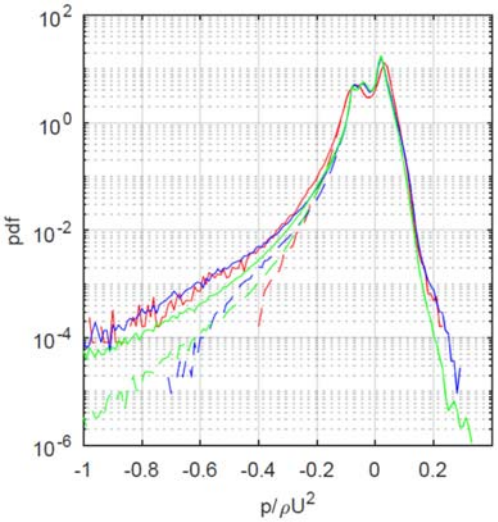

Figure 2: Probability distribution function of pressure in wake of a Schiebe body (Arndt et al., 2009), for three grid discretization levels. Dashed lines correspond to DES simulations, solid lines to corrected values using deterministic model. Red lines correspond to refinement block, coarse grid, blue to medium and green to fine grid as shown in Table 1.

The figure shows that the negative-pressure side of the pdf of the resolved pressure is, once corrected, indeed exponential, which is consistent with the probabilistic model for the unresolved pressure fluctuations.

2.3 Frequency of cavitation events

The previous two sections describe how, starting from a LES solution, the resolved pressure field is updated to improve the prediction of low pressure regions both deterministically and probabilistically to include sub-grid fluctuations. The second requirement for a cavitation inception model is to translate the pressure signal into a frequency of cavitation events.

Multiple different approaches can be considered. If the sub-grid fluctuations are ignored, the simplest possible model relies on tallying the number of events per simulated second, with an event being a region where the pressure (resolved, or deterministically corrected) is lower than the vapor pressure. This approach is straightforward to implement, but ignores important processes such as the duration of the low pressure burst and the dynamics of the nuclei. It also does not consider the size of the cavitating region, which has practical implications for detectability.

A difficulty of basing the calculation on the detection of a zone of low enough pressure is that that condition in itself does not quantify the extent of the cavitation event. A better model can be developed by considering the flux of nuclei into regions where pressure is low enough for cavitation to occur. This approach naturally incorporates the probability of nuclei being present and accounts for the volumetric extent of the cavitation region. Figure 3 shows schematically the proposed model. If a volume V_{cav} (t) is defined such that $p<p_{\mathrm{cav}}$ inside the volume, the flux of nuclei into the volume (and the frequency of cavitation events) is

$$f_{\mathrm{cav}}^{\mathrm{det}}(t) = \int_{S_{\mathrm{cav}}} N \min\left(\left(\boldsymbol{u_{Sp}} - u\right)\cdot \boldsymbol{n}, 0\right) dS, \quad (10)$$

where N is the nuclei density and $\boldsymbol{u_{Sp}} - u$ the relative velocity of the surface, with $\boldsymbol{u_{Sp}}$ and u the surface and fluid velocities, respectively. An equivalent and easier numerical implementation is to identify the set J(t) of computational nodes j that the surface traverses, defined by the condition

$$\{p(x_j,t) > p_{\mathrm{cav}}\} \,\&\, \{p(x_j,t) + \delta t D_t p(x_j,t) < p_{\mathrm{cav}}\} \quad (11)$$

with $D_t p$ the material derivative of p, and approximate

$$f_{\mathrm{cav}}^{\mathrm{det}}(t) = \textstyle\sum_{j\in J(t)} N V_j \,/\delta t. \quad (12)$$

This deterministic model produces satisfactory results if the solution has sufficient resolution, but a model that incorporates the probability distribution of the sub-grid fluctuations is required for most simulations with LES resolutions. A possible model based on the distribution presented in Eqn. (4) simply assigns to each node in the computational domain a probability of cavitation events equal to the cdf for $p<p_{\mathrm{cav}}$ divided by a characteristic cavitation time, i.e.,

$$f_{\mathrm{cav}}^{\mathrm{prob}}(t) = \textstyle\sum_j N V_j C((p_{\mathrm{cav}} - p(x_j,t))/\rho u'^2)\,/\tau_{\mathrm{cav}}. \quad (13)$$

While this is somewhat arbitrary, the rationale is that there is a maximum frequency of isolated events that can occur at a location, which are related to the time required for a bubble to grow. Since the purpose of this model is the characterization of inception processes, it is expected that

it is applied for conditions where these events are detectable, but not too frequent. Temporal and volumetric integration in the region under observation, considering a nuclei number density, results in the final probabilistic inception frequency.

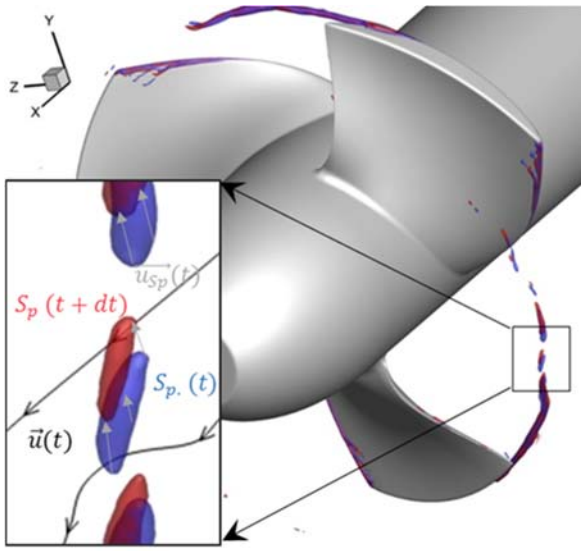

Figure 3: Schematic representation of proposed deterministic integration method, based on a LES solution for P5206. Blue iso-surfaces correspond to region of pressure below vapor pressure at time t, red regions at t+Δt; black streamlines are fluid velocity, grey represents the velocity of the pressure contours.

3 CFD SIMULATIONS

3.1 Solver

The code REX, developed at the University of Iowa, was used for all simulations, and auxiliary post-processing tools were developed to correct pressure distribution in the discrete solutions as discussed in the previous section. The most up to date description of the solver can be found in Li and Carrica (2018) and references therein. REX is a general purpose CFD solver, for which multiple models of turbulence have been implemented. Results presented herein used DDES turbulence model based on Menter's SST $k-\omega$ model, as well as standard and dynamic Smagorinsky LES models. Results indicated as RANS correspond to SST model without the DES extension. Note that the wall spacing resolution is insufficient to properly resolve the smallest scales in the boundary layer, however the regions of interest are in wake regions where the model's assumptions are valid. The convection terms in the equations are discretized with fourth order upwind biased differences for momentum and second order for other quantities. Diffusion and temporal terms use second order central and second order backwards schemes, respectively.

3.2 Grid and Simulation Conditions: Waterjet propulsion system

The waterjet driven axisymmetric body studied experimentally by Arndt et al. (2009) was simulated for several jet velocity ratios. The experimental Schiebe body has a diameter of 0.03 m with a length of 0.241 m, and the jet orifice has diameter of 3.75×10^{-3} m. The computational domain has been discretized by three overset grids as presented in Table 1 and shown in Figure 4. Three levels of refinement were considered, with a systematic refinement factor of 2.

Several experimental conditions, characterized by the ratio of the jet velocity U_j to the free stream velocity U, were simulated. DDES method was mainly used for this study, however one solution using RANS is also included. Statistically stationary conditions behind the jet driven body are ensured before analyzing inception.

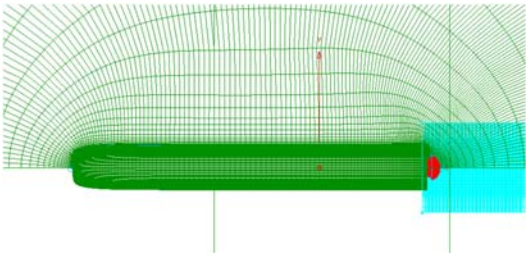

Figure 4: Schiebe body grid system with three overset grids. (1. Background (Green) 2. Jet (Red) 3. Refinement (Blue))

Table 1: Grid dimensions for Schiebe body simulations.

	Dimensions		
	Background	Jet	Refinement
Fine	301x91x361	151x91x61	301x181x181
Medium	151x46x181	76x46x31	151x91x91
Coarse	76x24x91	39x24x16	76x46x46

3.3 Grid and Simulation Conditions: DTMB 5206

The ducted propeller DTMB 5206, experimentally studied by Chesnakas and Jessup (2003), is the second example considered. The propeller, shown in Fig.3 without its duct, is three-bladed, with constant chord of 0.3812 m, a tip diameter of 0.8503 m and a duct diameter of 0.8636m. The documented $J = 0.98$, $n = 500$ rpm condition is used in all simulations. Inception and full cavitation were documented at $\sigma = 11$ and 5.6, respectively. Interestingly, the reported location of cavitation inception is approximately half a chord downstream from the blade trailing edge, while full cavitation occurs closer to the blade, both in the leakage and trailing edge vortices. Chesnakas and Jessup (2003) hypothesized that cavitation was controlled in this case by the merger of these two vortices, that can sporadically result in large negative pressure fluctuations. While the merger occurs closer to the blade than half a chord, given the very large velocities and the typical growth time of a cavitating bubble, it is possible that the detection location takes place further downstream.

A coarse grid (Fig. 5) and a fine grid were considered for the discretization of the case, with a refinement factor of 2 between the two for most blocks; the number of grid points is respectively 39.7M and 153M. For the fine case, while all the body-fitted grids were refined, only one of the blades uses the finest refinement to reduce the computational cost. This introduces some asymmetry to the solution but it is not expected to significantly affect the

region of interest. The refinement blocks in the regions of interest have near unit aspect ratio to ensure good quality results for the LES method, and the time step is such as to have a CFL number less than one in this region. In practice, a time step equivalent to an eighth of a degree of rotation of the propeller was used for the fine grid, and a quarter of a degree for the coarse grid.

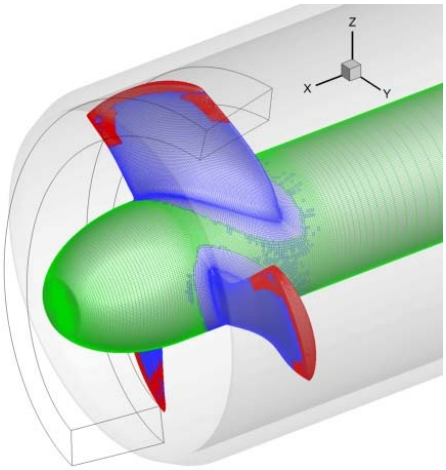

Figure 5: Grids for P5206 (coarse grid); duct wall is shown as a translucent surface and only one of the local blade tip refinements is shown for clarity.

4 RESULTS AND DISCUSSION

4.1 Waterjet propulsion system

The prediction of cavitation inception of the flow has been performed for a free stream velocity of 10 m/s for a series of jet velocity ratios. The onset of cavitation inception is observed in the wake of the body for low jet velocity ratio and at the jet for high jet velocity ratio (in the mixing layers), in agreement with experiments. Examples of the two conditions are shown in Figure 6.

The predicted inception index is compared against the experimental values for three grids in Figure 7 for U_j/U =1.5. An event frequency of 10 Hz is used as criterion for inception. This result shows that using the pressure as-computed leads to an under-estimation of σ_i, the inception cavitation number defined as $\sigma_i = 2(p - p_{cav})/\rho U^2$. This error becomes less important as the grid is refined. The proposed correction of the core pressure, which decreases as the grid is refined, improves the prediction. However improvements in the estimation are still needed to obtain a prediction that is not grid dependent. The probabilistic correction based on R_λ has a much smaller effect in σ_i for this case, likely due to modest levels of R_λ. An additional point for a RANS only simulation is included. The value has been corrected using the probabilistic approach outlined in §2.1; though the assumption that unresolved fluctuations follow the pdf of IHT is less justifiable for RANS. The result is comparable to those from DDES, which is promising when considering much lower computational cost of RANS. The probabilistic approach produces a larger correction for RANS, since R_λ is also larger.

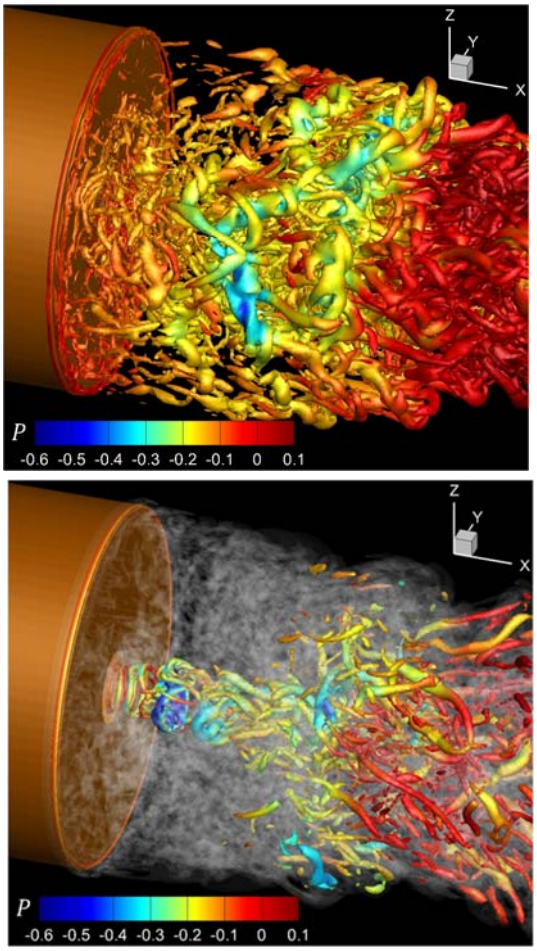

Figure 6: Q-criterion for instantaneous flow for U_j/U=0 (top) and U_j/U=1.5 (bottom). Uncorrected pressure given as $P=p/\rho U^2$

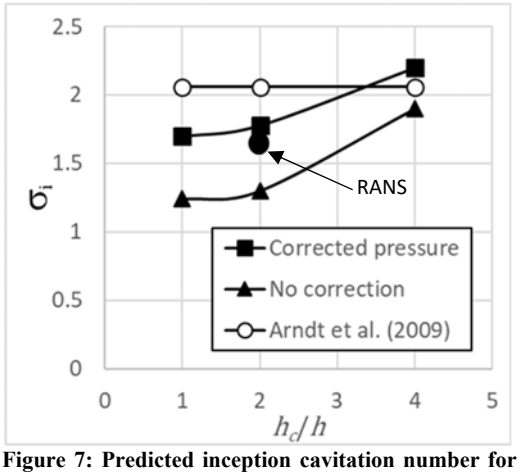

Figure 7: Predicted inception cavitation number for U_j/U=1.5, as a function of grid size h; h_c is the characteristic grid size for the coarse case. Corrected cases include IHT and core corrections. All simulated cases use DDES, except noted result for RANS.

4.2 DTMB 5206

Results for ducted propeller DTMB 5206 using multiple turbulence models are presented herein. The simulated flow fields are in general good agreement with the experimental results of Chesnakas and Jessup (2003), and other available numerical efforts such as Hsiao and Chahine (2004). Figure 8 shows an instantaneous flow field for LES (fine grid). It shows clearly that a region of low pressure occurs as the leakage vortex and a second vortex originating at the trailing edge on the pressure side of the blade interact. At this level of fine discretization, CFD can predict low enough pressures as observed experimentally for inception conditions. In the most basic approach, the presence of low pressure events can be considered sufficient to indicate inception; however the objective of the proposed models is to better quantify the probability of detecting such events requiring the computation of a frequency of detection.

Figure 9 compares the same region of the flow across the considered turbulence modeling methods. Besides the increased resolution of small structures as the method′s fidelity is increased from RANS to DDES to Dynamic Smagorinsky LES, and from coarse to fine resolution for the latter, the main difference observed is that RANS predicts a more separated leakage vortex, resulting in a delayed interaction with the trailing edge vortex, and a prediction of a region of low pressure further away from the blade. LES results show, even for uncorrected pressure fields, low values in the range C_p= [-8, -10], and as described previously, sporadically even lower for the fine grid case. Outside the boundary layers, where the proposed correction to pressure is not valid, the recovered pressure deficit is limited to the core of the vortices, which are clearly observed using *d*-criterion (Eq. 8). Remarkably, the chosen value of *d* is comparable with the grid size, which in the region of interest is $\Delta = 2.5 \times 10^{-3} R$ (coarse) and $1.25 \times 10^{-3} R$ (fine), indicating that *d* is indeed a good approximation of the local radius from the core of each vortex.

The comparison of fine and coarse LES results is illustrative of the amount of small structures being modeled at the sub-grid scale in the coarse case. Deterministic pressure corrections in the range $C_{\Delta p}$= [0.5, 1.5] are observed in the strongest vortices for both coarse LES and DDES, but more modest corrections occur in the other two cases. In RANS, this is due to a poorer resolution of vortical structures; while in fine LES it is a consequence of better resolution of the vortices and to breakup into smaller structures. Note also in Figs. 8 and 9 that the regions of low pressure are much smaller than the regions of high vortex concentration. In regions outside the leakage vortex, the "surface" of the vortices, as defined by *Q*, have too large pressure values to be good candidates for cavitation regions. Finally, it is important to mention that, as in previous numerical efforts, the location of the minimum pressure appears closer to the blade tip than the reported experimental value. A possible reason for this discrepancy is that a model based exclusively in fluid variables, such as the one presented here, cannot account for nuclei dynamics and transport that can affect the detection location.

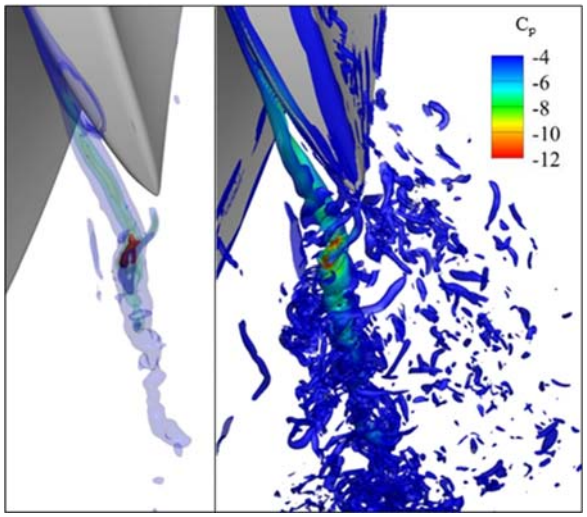

Figure 8: Instantaneous LES solution for P5206. Left: iso-surfaces of pressure (uncorrected); right: Q-criterion. All surfaces colored with pressure coefficient. Regions with C_p < -11,, equivalent to experimental inception conditions, are shown as solid red surfaces in left panel.

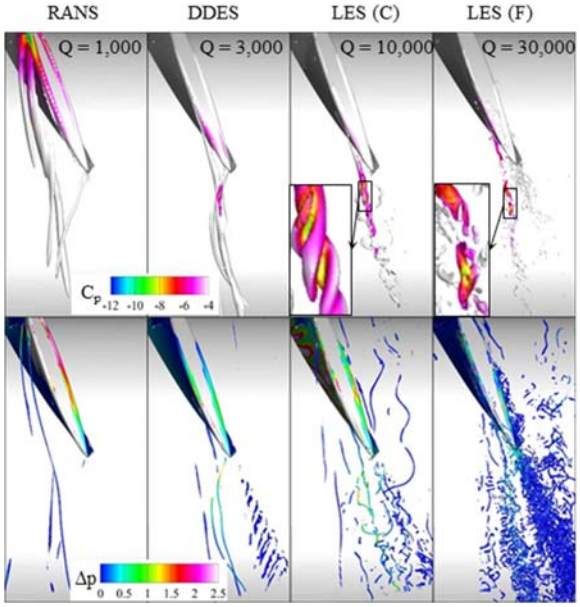

Figure 9: Comparison of instantaneous flow structures for different methods. All panels except rightmost ones correspond to coarse grid. Q-criterion surfaces at indicated level are shown in top row, d-criterion iso-surface d=0.0035R is shown in lower row. Low pressure areas in LES solutions shown in inserts.

The proposed models were applied to determine the frequency of observable events for different reference pressures. The inception cavitation number is defined as $\sigma_i = -C_p$ in the following discussion. The current models can also provide the spatial distribution of the frequency of events, as shown in Figure 10. The regions of non-negligible probability of detection are highly concentrated

for this case, as opposed to the previous case for which low pressure events can occur more randomly. The predicted density levels differ between the two methods due to the choice of a prescribed cavitation time of 0.02 s for the probabilistic method. This time is chosen as the characteristic time between two cavitation events at a given location, and is likely case dependent. Without further information to guide the selection of a value for this particular application, at this time is chosen as a reasonable order of magnitude value.

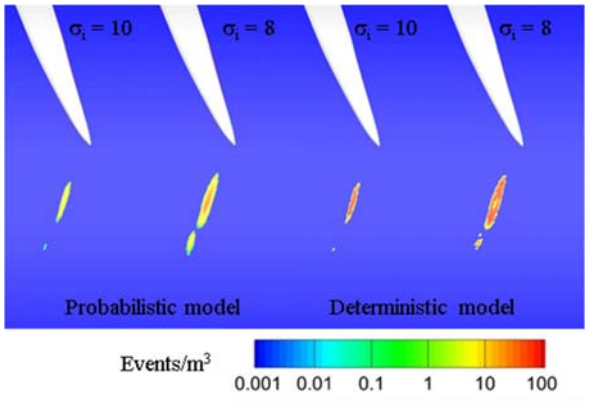

Figure 10: Density of detectable events as a function of reference pressure and model. Computation used DDES model. Reference σ_i and pressure correction method indicated for each case.

Figure 11 presents the integrated predicted rates of events for the different simulations considered. The series, particularly for the LES cases, are relatively short, due to the cost of the simulations and this might affect the final statistics, by under- or over-representing extreme events. A consistent method of evaluating the length of a temporal series for cavitation analysis is part of the on-going work.

Experimentally, the reported detection rate considered representative of inception conditions is 1 event every ten seconds as observed with a stroboscopic light at the propeller rotation rate of 8.33 Hz (Chesnakas and Jessup, 2003), which is reported to occur at $\sigma_i = 11$. An equivalent frequency can be estimated based on the reported duration of a cavitating burst of 0.5 ms and the propeller rotational speed as 16.66 Hz. The nuclei density considered is N = 10^7 particles/m^3. The analysis shows that without incorporating the deterministic pressure correction only LES for the fine grid predicts inception at $\sigma_i = 11$ or higher, with all the other methods predicting a value in the range 7-9. Interestingly, the predictions of RANS and DDES are very similar. A possible reason for this behavior is that the cavitation occurs close to the duct wall and for the hybrid method RANS effects can be significant in this region. This is supported by the strong differences between DES and LES flow features, as shown in Fig. 9.

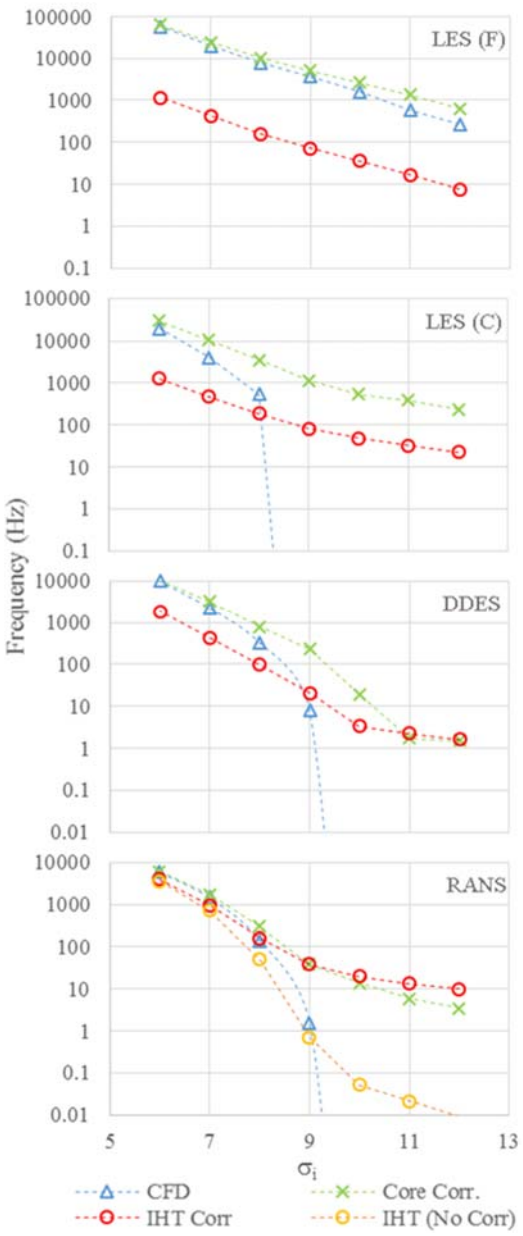

Figure 11: Predicted frequency of cavitation events for P5206, for different turbulence models and grid discretization. Blue symbols are for pressure fields as provided by the solver, green using deterministic core correction (§2.2) and red with both deterministic and probabilistic corrections (§2.1 and §2.2). For RANS probabilistic correction without core correction is also included.

The deterministic correction (in green in Fig 11) is sufficient to predict frequencies of events larger than 1 Hz for all methods at $\sigma_i = 11$. The correction has the most significant effect at very low pressures, as a combination of those pressure events being rare and also most energetic, resulting in a larger correction than for weaker vortices. RANS results were also included since the main steady structure from the leakage vortex and the trailing vortices are well captured, but in general this correction should have

little relevance for the RANS method. Finally, by comparing coarse and fine LES results, it is clear that the correction is able to reduce the gap between the two grid resolutions, so that for all σ_i both predictions are within a factor of 5 of each other.

The probabilistic correction has little effect in this case, as previously discussed, due to the localized (i.e., deterministic) nature of the low pressure regions. For the RANS simulation only, the probabilistic correction was calculated without correcting the vortex core pressure to illustrate the strong effect in the very low pressure range.

While overall the results are encouraging and produce estimates that compare favorably with the experimental data, some of the limitations of the current model are evident from these results. The fine LES case, which should require less modeling, predicts the highest frequency, of about 1,000 Hz at $\sigma_i = 11$. In contrast, the same data but with the event rate limited to 50 Hz at any given location (probabilistic model), gives a frequency similar to the estimated experimental one. This clearly indicates that the cavitation-event count is over-predicting the cavitation capacity of the system, by counting low-pressure events that are too short to generate a viable cavitation event. The absence of a clear drop-off as observed in the coarser grids is also likely due to an over-estimation of the duration of the extremely low pressure events, which are shorter than those at higher values. It is expected that consideration of the nuclei dynamics can correct these effects.

5 CONCLUSIONS AND FUTURE WORK

A general framework for cavitation inception modeling based on a probabilistic approach has been presented. The model attempts to recover low pressure events that are under-estimated by underresolved CFD mainly due to two reasons: discretization errors at the vortex core and sub-grid modeling of unresolved fluctuations. Further improvement of the model is certainly necessary to reduce grid dependence, which is suspected to originate mainly from the vortex core correction and low pressure event duration.

The probabilistic method as currently implemented relies on the dependence of the sub-grid fluctuations on the Taylor microscopic Reynolds number. It is based on a limited dataset of pdfs that correspond to a few moderate values of R_λ. For typical cases of interest, this leads to unverified extrapolations of the pdfs towards higher R_λ, especially in RANS regions of the domain. While the model is primarily intended to be used with the hybrid RANS/DDES approach, for which the IHT sub-grid assumption is reasonable, the possibility of the region of interest for cavitation being in the RANS regions needs to be considered. The improvement of the model for higher R_λ and the implementation of alternative models for regions where IHT is a poor approximation of the unresolved flow are all areas of future work.

The current implementation ignores nuclei dynamics, assuming simply a uniform distribution of particles. This assumption decouples the fluid dynamics problem from the nuclei dynamics, but contributes to uncertainty in the estimation of the cavitation inception number. Hsiao and Chahine (2004) clearly showed that bubble dynamics must be included to account for growth time, which can result in non-negligible displacement in the typically fast environments of interest. Besides the inclusion of bubble dynamics in a deterministic fashion, work is on-going with the objective of including the nuclei dynamics via the Rayleigh-Plesset equation at the sub-grid scale model.

6 AKNOWLEDGEMENTS

This research was sponsored by the US Office of Naval Reseach through MURI grant N00014-17-2676, Univ. of Minnesota lead institution, Dr. Ki-Han Kim program officer. GB acknowledges financial support from FAPESP (Brazil), grant 2018/08752-5. Computations were performed at the DoD HPCMP systems Onyx and Centennial.

REFERENCES

Arndt, R.E.A, Amromin, E. L. & Hambleton, W. (2009). 'Cavitation Inception in the Wake of a Jet-Driven Body', J. Fluids Engineering, 131, 111302-1-8

Cao, N., Chen, S. & Doolen, G. D. (1999). 'Statistics and structures of pressure in isotropic turbulence', Physics of Fluids, 11:8, 2235-2250.

Chesnakas, C. J. & Jessup, S. D. (2003). 'Tip-vortex induced cavitation on a ducted propulsor', 4th ASME-JSME Joint Fluids Engineering Conference, Honolulu, HI, USA.

Hsiao, C.T. & Chahine, G. L. (2004). 'Numerical Study of Cavitation Inception due to Vortex/Vortex Interaction in a Ducted Propulsor', 25th Symposium on Naval Hydrodynamics, St. John's, Canada, 8-13 August.

Li, J., & Carrica, P. M. (2018). 'An approach to couple velocity/pressure/void fraction in two-phase flows with incompressible liquid and compressible bubbles'. International Journal of Multiphase Flow, 102, 77-94.

Pumir, A. (1994). 'A numerical study of pressure fluctuations in three-dimensional, incompressible, homogeneous, isotropic turbulence'. Physics of Fluids, 6, 2071.

Ran, B. & Katz, J. (1994). 'Pressure fluctuations and their effect on cavitation inception within water jets'. Journal of Fluid Mechanics, 262, 223-263.

Spalart, P.R. (1999). 'Strategies for turbulence modelling and simulations', 4th International Symposium on Engineering Turbulence Modelling and Measurements, Ajaccio, France, 24–26 May.